

Linear Response and Electron Transfer in Complex Biomolecular Systems and a Reaction Center Protein

Fabio Sterpone,[†] Matteo Ceccarelli,[‡] and Massimo Marchi^{*,†}

Commissariat à l'Energie Atomique, DSV-DBJC-SBFM, Centre d'Études, Saclay,
91191 Gif-sur-Yvette Cedex, France, and CSCS/ETHZ, Via Cantonale, CH-6928 Manno, Switzerland

Received: May 16, 2003; In Final Form: July 18, 2003

This paper is focused on the dielectric linear response in the context of electron-transfer reactions in complex biomolecules with and without explicit electronic polarization. Molecular dynamics simulation is used for a detailed investigation of two systems: a bacteriochlorophyll molecule in a homogeneous environment (liquid water) and a reaction center protein of bacterial photosynthesis in amphiphilic solution. The limits of the linear approximation and the size of its deviation from the results, in principle exact, obtained from thermodynamic integration are pinpointed. Our findings will be of crucial importance in further investigations of electron transfer in complex biomolecules making use of linear response, still the easiest and least time-consuming approach.

I. Introduction

Electron transfer (ET) plays a fundamental role in many chemical and biological processes.¹ In plants, algae, and bacteria, ETs between simple organic molecules (cofactors) arranged in the interior of protein complexes are a key element of the photosynthetic process. These transfers can be rapid, as fast as a few picoseconds, and highly specific.

The Marcus theory² explains the transfer between two redox sites as driven by spontaneous thermal fluctuations of the solvent. The reaction coordinate for the ET is a collective variable, the so-called energy gap, or E-gap, defined as the solvent electrostatic energy difference between the initial and final redox states. The Marcus approach is based on linear response and assumes a Gaussian probability distribution for E-gap.^{3,4}

Previous papers have shown that E-gap probability distributions are Gaussian in very complex systems such as molecular liquids (see, for instance, ref 4) and proteins.⁵ The central limit theorem can be invoked to explain this linear behavior, if the E-gap contains contributions only from two-body interactions and coupled multiple minima do not play a role.

This paper is concerned with donor–acceptor electron exchanges where electronic polarization, intrinsically a many-body effect, and conformational changes of the milieu play a significant role. In this case, one cannot expect the Gaussian behavior of the E-gap, and the free-energy surfaces for the E-gap must be computed directly. Umbrella sampling and a thermodynamic integration (TI) scheme can be used for this purpose.⁶ For ET problems, these techniques consist in gradually charging the system from its initial to final charge-separated state.

Electronic polarization, not routinely included in popular biochemical force fields, is essential to represent the anisotropy of the electrostatic interaction which is underestimated by fixed charge models (see, for instance, ref 7). In addition, the temperature dependence of the electrostatic interaction is badly

represented by nonpolarizable force fields. This is of crucial importance in biomolecules, as shown by recent results on simulation on folding of all atom–protein models.⁸

Although Simonson⁵ found that the dielectric response of Cyt c is linear to a good approximation. This cannot be easily generalized because large number of conformational microstates and multiple minima are known to exist in proteins.⁹ Indeed, in a recent study^{10,11} we found that in the reaction center (RC) protein of *Rhodobacter (Rb.) sphaeroides*, nonlinear coupling exists between the photosynthetic primary charge separation and conformational changes in the protein.

In this paper, we present an investigation of nonlinear effects induced on ET by electronic polarization and multiple minima in water solution and in a protein. First, we study the response to charging of a bacteriochlorophyll (a cofactor of bacterial photosynthesis) in water. Second, we compute the free-energy profiles to transfer an electron between two cofactors of the reaction center protein of *Rb. sphaeroides*. Anticipating our results, we find that electronic polarization has the largest effect on a highly anisotropic environment such as in proteins. Also, conformational motions coupled to ET are shown to have a large effect on the free-energy profiles, which limits the applicability of the Marcus theory.

The paper is organized as follows: section II describes the thermodynamic integration and umbrella sampling schemes used to obtain driving forces and free-energy profiles. Section III provides all simulation details and protocols, and results are presented and discussed in section IV. The paper ends with a conclusion.

II. Theoretical Framework

II.A. Electron Transfer and the Gaussian Approximation.

The Marcus theory uses a Gaussian model of the E-gap fluctuation to arrive to an analytical expression for the driving force and activation free energy.

For an electron transfer from a donor state, A, to an acceptor, B, immersed in a given solvent, the driving force, ΔG_{10} , is the difference in solvation free energy between a state 1 where the

* Corresponding author. E-mail: marchi@villon.saclay cea.fr.

[†] Commissariat à l'Energie Atomique.

[‡] CSCS/ETHZ.

electron is on B and a state 0 where the electron is on A. ΔG_{10} can be computed from a simulation using the expression:

$$e^{-\beta \Delta G_{10}} = \langle e^{-\beta \epsilon} \rangle_0 = \int d\epsilon \rho_0(\epsilon) e^{-\beta \epsilon} \quad (1)$$

Here, the symbol $\langle \dots \rangle_0$ indicates an ensemble average on state 0, ϵ is the energy gap or the electrostatic potential energy difference between states 1 and 0, and $\rho_0(\epsilon)$ is its probability distribution in state 0. It can be readily shown¹² that $\rho_0(\epsilon)$ and $\rho_1(\epsilon)$ are related by the expression:

$$\rho_1(\epsilon) = \rho_0(\epsilon) e^{-\beta \epsilon} e^{-\beta \Delta G_{10}} \quad (2)$$

Or in terms of free energies:

$$G_1(\epsilon) = G_0(\epsilon) + G_0(\epsilon) + \epsilon + \Delta G_{10} \quad (3)$$

If the distributions $\rho_1(\epsilon)$ and $\rho_0(\epsilon)$ are Gaussian, or, alternatively, if the free-energy $G_1(\epsilon)$ and $G_0(\epsilon)$ are harmonic, one can readily derive an expression for ΔG_{10} which reads:

$$\Delta G_{10} = \epsilon_0 - \frac{1}{2} \beta \sigma^2 \quad (4)$$

where ϵ_0 stands for the ensemble average of the energy gap in state 0 and σ is the Gaussian width of the probability distribution. Also, once the driving force is known, by using eq 3 the parabolic free-energy surfaces for states 0 and 1 can be obtained as:

$$G_0(\epsilon) = \frac{(\epsilon - \epsilon_0)^2}{2\beta\sigma^2} \quad (5)$$

$$G_1(\epsilon) = \frac{(\epsilon - \epsilon_1)^2}{2\beta\sigma^2} + \epsilon + \Delta G_{10} \quad (6)$$

The activation free-energy ΔG^* corresponds to the crossing point of the two surfaces, and in this Gaussian approximation is equal to:

$$\Delta G^* = \frac{\epsilon_0^2}{2\beta\sigma^2} \quad (7)$$

By introducing the system reorganization energy $\lambda_r = 1/2 \beta \sigma^2$ and using eq 4, we obtain the familiar Marcusian expression for the activation energy:

$$\Delta G^* = \frac{(\Delta G_{10} + \lambda_r)^2}{4\lambda_r} \quad (8)$$

Thermodynamic integration and umbrella sampling^{13,14} can be used to verify and test the Gaussian approximation capability to compute the driving force and the free-energy profiles of the redox exchange.

II.B. Thermodynamic Integration. The scheme implies a series of calculations on a set of ensembles connecting, in a thermodynamic sense, the initial and final states. The thermodynamic path is generated by modifying the atomic charges of the two redox centers. For each atom i th in the acceptor or donor, one can write:

$$q_i(\lambda) = q_i(0) + \lambda[q_i(1) - q_i(0)] \quad (9)$$

where $q_i(0)$ and $q_i(1)$ are the charges of the i th atom in states 0 and 1, respectively. Here, λ is a control parameter which takes

values in the interval [0,1]. The corresponding free energy of the transformation, or driving force, is evaluated using the following relation:

$$\Delta G_{10} = \int_0^1 d\lambda \left\langle \frac{\partial U(\lambda)}{\partial \lambda} \right\rangle_\lambda \quad (10)$$

where $U(\lambda)$ is the electrostatic potential energy in the intermediate state λ . The same procedure can also be used to compute the solvation free energy of charging of a single molecule. Then, this free energy corresponds to an oxidation or to a reduction process, depending on the sign of the excess charge.

Following the spirit of the Marcus theory, one is interested only in computing the contribution of the solvent to the electrostatic potential acting on the redox sites. Consequently, the potential energy $U(\lambda)$ excludes all of the charge–charge interactions within each of the redox sites. This internal contribution to the free-energy difference is approximated by the gas-phase difference between the energies of ionization and affinity of the redox sites.

When the computation model for the solvent and the redox centers does not include electronic polarization, the integrand in eq 10 has a simplified expression since the electrostatic potential at a generic thermodynamic point can be expressed by the interpolation formula:^{5,15}

$$\bar{U}(\lambda) = \bar{U}(0) + \lambda[\bar{U}(1) - \bar{U}(0)] \quad (11)$$

$$\left\langle \frac{\partial \bar{U}(\lambda)}{\partial \lambda} \right\rangle_\lambda = \langle \bar{U}(1) - \bar{U}(0) \rangle_\lambda = \langle \epsilon \rangle_\lambda \quad (12)$$

The bar symbol means that internal interactions are excluded for each redox site. When electronic polarization terms are added a posteriori via induced dipoles μ , we cannot express $\bar{U}(\lambda)$ as in eq 11 (see section II.D. and ref 11). In this case, the potential energy terms involving dipoles, charge–dipole, and dipole–dipole cannot be separated into a combination of final and initial states. Thus, at each instant of the trajectory the partial derivative of the potential energy can be written as:

$$\frac{\partial U(\lambda)}{\partial \lambda} = \sum_i \frac{\partial U(\lambda)}{\partial q_i} \frac{\partial q_i}{\partial \lambda} + \frac{\partial U(\lambda)}{\partial \mu_i} \frac{\partial \mu_i}{\partial \lambda} \quad (13)$$

As discussed in ref 11, the atomic-induced dipoles are obtained by a self-consistent iterative procedure which at convergence imposes the condition $\partial U / \partial \mu_i = 0$. It follows that eq 13 can be rewritten as:

$$\frac{\partial U(\lambda)}{\partial \lambda} = [U^{qq}(1) - U^{qq}(0)] - \sum_i [\mathbf{E}_i^{qq}(1) - \mathbf{E}_i^{qq}(0)] \cdot \mu_i^\lambda \quad (14)$$

where the suffix qq refers to the charge–charge interactions and \mathbf{E}_i^{qq} is the total electric field acting on the atom i . By eliminating the interaction terms internal to each redox center, eq 14 can be used to compute the statistical average $\langle \partial U(\lambda) / \partial \lambda \rangle_\lambda$ in eq 10.

II.C. Free-Energy Surfaces and Umbrella Sampling. Umbrella sampling, or US, is a popular technique used to compute potentials of mean force in condensed phase.^{13,14} The same technique has also been used to obtain the free-energy surfaces for electron exchange from classical simulations (see, for instance, ref 12 and references therein). As in the case of TI, trajectories are generated in ensembles obtained by charging

up (or down) the redox sites using eq 9. Umbrella sampling then computes the probability distribution in the reference ensemble, the initial state 0, of the reaction coordinate $\epsilon(\mathbf{R})$ (i.e., the energy gap for the system coordinates \mathbf{R}) by unbiasing the probability distribution sampled in any λ ensemble by:

$$\langle \rho(\epsilon) \rangle^{\text{unbiased}} = \frac{\langle \delta(\epsilon(\mathbf{R}) - \epsilon) e^{\beta(U_\lambda - U_0)} \rangle_\lambda}{\langle e^{\beta(U_\lambda - U_0)} \rangle_\lambda} \quad (15)$$

This equation cannot be used as is, since the ensemble average of the exponential $e^{\beta(U_\lambda - U_0)}$ is highly oscillatory. The trick is to replace $(U_\lambda - U_0)$ by a function of $\epsilon(\mathbf{R})$. This is possible in the simple case where $U_1 - U_0$ is the energy gap, giving:

$$e^{\beta(U_\lambda - U_0)} = e^{\beta\lambda\epsilon(\mathbf{R})}$$

Unfortunately, for the redox centers we are interested in (large bacteriochlorophyll molecules) and for a model with no electronic polarization, the reaction coordinate is $\epsilon(\mathbf{R}) = \bar{U}_1 - \bar{U}_0$, where the electrostatic potential, \bar{U} , does not include electrostatic contributions internal to the redox centers.

To obtain a manageable expression for eq 15, we first notice that the potential U can be decomposed in two terms: One depending explicitly on the reaction coordinate, $\epsilon(\mathbf{R})$, and another responding only to a restricted set of configurational space coordinates, the internal coordinates of the chromophores or $\hat{\mathbf{R}}$. We can write:

$$U(\lambda, \mathbf{R}) - U(0, \mathbf{R}) = \bar{U}(\lambda, \mathbf{R}) - \bar{U}(0, \mathbf{R}) + \chi(\hat{\mathbf{R}}) = \lambda\epsilon(\mathbf{R}) + \chi(\hat{\mathbf{R}}) \quad (16)$$

We have tested, for our particular case, that the two terms are statistically independent. Indeed, in solvated bacteriochlorophyll, internal chromophore motions are decoupled of the energy gap, probably because of their intrinsic rigidity. We find that the computed $\langle \delta\epsilon(\mathbf{R}) \delta\chi(\hat{\mathbf{R}}) \rangle$ is small compared to $\langle \epsilon(\mathbf{R}) \chi(\hat{\mathbf{R}}) \rangle$ in any ensemble of the umbrella procedure; the relative error is always less than 0.03%. Because of this independence, the combined probability distribution for ϵ and χ can be factorized into:

$$P(\epsilon, \chi) \approx P(\epsilon)P(\chi) \quad (17)$$

At the same time, any ensemble average $\langle f(\epsilon) f(\chi) \rangle$ can be computed as:

$$\langle f(\epsilon) f(\chi) \rangle = \int d\epsilon d\chi f(\epsilon) f(\chi) P(\epsilon, \chi) \quad (18)$$

$$\approx \int d\epsilon P(\epsilon) f(\epsilon) \int d\chi f(\chi) P(\chi) \quad (19)$$

By substituting eq 16 into eq 15 and using eq 19, $\langle \rho(\epsilon) \rangle^{\text{unbiased}}$ can be rewritten as:

$$\langle \rho(\epsilon) \rangle^{\text{unbiased}} \approx \frac{\langle \delta(\epsilon(\mathbf{R}) - \epsilon) e^{\beta\lambda\epsilon(\mathbf{R})} \rangle_\lambda \cdot \langle e^{\beta\chi(\hat{\mathbf{R}})} \rangle_\lambda}{\langle e^{\beta\lambda\epsilon(\mathbf{R})} \rangle_\lambda \cdot \langle e^{\beta\chi(\hat{\mathbf{R}})} \rangle_\lambda} \quad (20)$$

$$= \frac{e^{\beta\lambda\epsilon} \langle \rho(\epsilon) \rangle_\lambda}{\langle e^{\beta\lambda\epsilon(\mathbf{R})} \rangle_\lambda} \quad (21)$$

When electronic polarization is included, $\epsilon(\mathbf{R})$ now contains contributions from charges and induced dipoles. As before, one can write $U(\lambda, \mathbf{R}) - U(0, \mathbf{R})$ as:

$$U(\lambda, \mathbf{R}) - U(0, \mathbf{R}) = \lambda\epsilon(\mathbf{R}) + \chi'(\mathbf{R}) \quad (22)$$

where $\chi'(\mathbf{R})$ now contains contributions from internal coordinates of the chromophore—still not included in the calculation of $\epsilon(\mathbf{R})$ —and from second-order terms in $\epsilon(\mathbf{R})$. As in the static charges case, we find that the two terms are well-uncorrelated with each other and in all our calculations the ratio $\langle \delta\epsilon(\mathbf{R}) \delta\chi'(\mathbf{R}) \rangle / \langle \epsilon(\mathbf{R}) \chi'(\mathbf{R}) \rangle$ is less than 0.1%.

The expression in eq 21 allows us to obtain the unbiased probability distribution of the reaction coordinate E-gap for each ensemble λ . To obtain the probability distribution in the ensemble $\lambda = 0$, the $\langle \rho(\epsilon) \rangle_{\lambda i}^{\text{unbiased}}$ for each ensemble $\lambda = \lambda_i$ needs to be appropriately matched. In our study, matching errors are minimized by the iterative procedure called WHAM.¹⁶ In this context, the final distribution probability of E-gap is:

$$\langle \rho(\epsilon) \rangle_0 = \sum_{i=1}^{N_w} \langle \rho(\epsilon) \rangle_{\lambda i}^{\text{unbiased}} \cdot \left[\frac{n_i e^{-\beta(\lambda_i \epsilon - G_i)}}{\sum_{j=1}^{N_w} n_j e^{-\beta(\lambda_j \epsilon - G_j)}} \right] \quad (23)$$

where n_i is the number of independent data points used to construct the biased distribution in the λ_i ensemble, N_w is the number of windows in the US procedure (in our case, it corresponds to the thermodynamic points of the procedure), and $e^{-\beta G_i} = \langle e^{\beta\lambda_i \epsilon} \rangle_{\lambda i}$.

II.D. Electrostatic Models for the Energy Gap. In our model, only electrostatic forces act on the exchanging electron. The dielectric response of the environment surrounding the redox centers is due to both nuclear and electronic polarizations. To compute $\epsilon(\mathbf{R})$ we include contributions from fixed charges and from polarizable dipoles. For the latter, we use a polarizable model due originally to Thole¹⁷ and applied by us to electron transfer in a previous investigation.¹¹ All the technical details for the calculation of the energy gap are fully described in ref 11. Briefly, the electronic polarizable model involved a set of isotropic polarizabilities distributed on all the atoms of the system.¹⁸ This polarizable model is applied in our study a posteriori on trajectories generated by a classical fixed charge model. At each point of the analyzed trajectory, the induced dipoles were computed by self-consistent iterations. The electric field due to fixed charges and induced dipoles was computed using a version of the smooth particle mesh Ewald technique.¹⁹

As done in ref 11, ESP (ElectroStatic Potential fit) charges were rescaled by a factor of 0.8 to remove the implicit electron polarization term now treated explicitly.

III. Simulation Details

The results discussed in this paper were obtained by carrying out classical molecular dynamics (MD) simulation on two systems: a hydrated bacteriochlorophyll, or BChl, and a RC protein of *Rb. sphaeroides* embedded in a micelle-like structure of lauryl dimethyl amino oxide (LDAO) in water. The E-gap history was computed via electrostatic calculations on the MD trajectories.

III.A. Bacteriochlorophyll Molecule in Water. To study the charging process of a chromophore in a homogeneous solvent, we simulated BChl in a cubic box of water of 30 Å per side and containing 827 TIP3²⁰ water. For simplicity, the isoprene tail was removed from the simulated BChl. An ab initio force field developed by us²¹ was used to describe the interactions involving the BChl molecule. All the simulations discussed in this paper were performed with the program ORAC²² in the canonical NVT ensemble at temperatures of 300 and 200 K. The electrostatic interactions were computed using

TABLE 1: Free Energy of a Positively and Negatively Charging Bacteriochlorophyll Molecule in TIP3P Water^a

models	ϵ	σ_0^2	ΔG_{Gauss}	ΔG_{TI}	$ G_{\text{TI}} - G_{\text{Gauss}} $
BChl-1 (\mathcal{G})	-30.3	32.9	-57.8 \pm 3.6	-54.7 \pm 0.6	3.1
BChl-2 (\mathcal{G})	-32.5	25.5	-54.0 \pm 2.7	-53.1 \pm 0.6	0.9
BChl-1 ($\mathcal{G} + \mathcal{D}$)	-34.3	20.0	-51.0 \pm 2.4	-55.6 \pm 0.6	4.6
BChl-2 ($\mathcal{G} + \mathcal{D}$)	-37.0	16.7	-50.3 \pm 2.1	-53.9 \pm 0.6	3.6
BChl-1 (\mathcal{G}) ^b	-0.7	32.9	-28.2 \pm 3.0	-26.4 \pm 0.6	1.8
BChl-1 ($\mathcal{G} + \mathcal{D}$) ^b	-6.5	19.0	-22.5 \pm 2.1	-28.3 \pm 0.6	5.8
BChl-1 200 K (\mathcal{G})	-25.0	24.6	-55.0 \pm 6.0	-55.3 \pm 1.5	0.3
BChl-1 200 K ($\mathcal{G} + \mathcal{D}$)	-30.6	15.3	-50.0 \pm 4.5	-57.2 \pm 0.9	7.2

^a ϵ and σ_0 were the Gaussian parameters, the mean and width, respectively, obtained by block averages. BChl-1 and BChl-2 are the charge distribution model discussed in the text. The labels (\mathcal{G}) and ($\mathcal{G} + \mathcal{D}$) indicate the fixed charge and the electronic polarizable models, respectively. Statistical errors were obtained by block averages and are 3 times the standard deviation. ^b Results for the cation BChl⁺. All remaining data are for charging the anion BChl⁻.

the SPME method²³ with convergence parameters chosen to maintain the error in the electrostatic energy below 0.01 kcal mol⁻¹.

The solvation free-energy calculations were carried out by TI. The whole process of charging consisted of nine intermediate ensembles, where the total charge of the molecule was increased from 0 (the neutral initial state) to -1 e with steps of -0.1 e each. For each thermodynamic point, the simulation was started from a configuration generated by the previous thermodynamic step. Then, the system was equilibrated for 50 ps and finally run for a further 500 ps. Configurations were saved every 240 fs.

Two different electronic distributions were used to represent the final charged state called BChl-1 and BChl-2. In the distribution BChl-1, in the text also referred to as uniform, the electron is equidistributed on the 16 atoms of the macroring: four nitrogens, four methine carbons connecting the rings, and eight methine carbons bound to nitrogens. BChl-2 was obtained by ab initio DFT calculations and fully described in ref 11.

III.B. Electron Transfer in a Reaction Center Protein. To study electron transfer in the RC of *Rb. sphaeroides*, we used an initial configuration of the RC protein, LDAO detergent, and water generated in our previous study on the primary charge separation.¹¹ All simulations were carried out in the NPT (constant temperature and pressure) ensemble at $T = 300$ K and $P = 0.1$ MPa, using identical simulation parameters and force field as described in ref 11 to which the interested reader is referred to for details.

In the present study, we have focused only on the transfer between the special pair (P) and the accessory of the L-side (B_L). This charge transfer is obtained through four intermediate steps. The electron is progressively removed from P and, at the same time, added to B_L. At each step, λ of eq 9 is increased by 0.2. As for the simulation of the hydrated BChl, each simulation of the TI path was started from a configuration generated by the previous thermodynamic step. Then, the system was equilibrated for 100 ps and finally run for a further 300 ps. New configurations were accumulated every 240 fs.

Two different distributions of the final state were used to generate the TI path. In the first, referred to as RC-1, we used uniform distributions for P⁺ and B_L⁻. For P, composed of two bacteriochlorophylls, we subtracted homogeneously half an electron from the 16 atoms of the macroring of each monomer. In the second distribution, named RC-2, we combined the uniform distribution for P⁺ and the DFT distribution for B_L⁻ described in refs 10 and 11.

IV. Results

IV.A. Bacteriochlorophyll in Water. The Gaussian approximation as described in section II.A. has been successfully

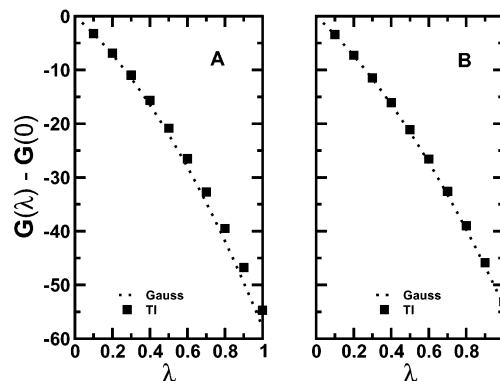


Figure 1. Free energy of solvation as a function of the charging parameter λ . Results from thermodynamic integration (TI): square symbols, and Gaussian approximation (Gauss): dotted lines. Panels A and B were obtained with charge distributions BChl-1 and BChl-2, respectively. All energies are given in kcal mol⁻¹. All results refer to the fixed charge model.

applied to systems where only one localized potential well affects the statistics of the energy gap. This was found to be the case for simple ions in solution^{15,24} and for chromophores in electron-transfer proteins.⁵ On the contrary, when the energy gap statistics are driven by more than one strongly coupled potential well, the approximation breaks down as demonstrated for the solvation of water.²⁵

We show in Table 1 the results for the solvation free energy to charge negatively and positively BChl in water. We first notice that the free energies computed with fixed charges (labeled \mathcal{G} in the table) are Gaussian. Indeed, for both charge distribution models (BChl-1 and BChl-2) the free energies computed with TI (ΔG_{TI} in the table) are within the error bar of their Gaussian approximations (ΔG_{Gauss}). Figure 1 shows that $G(\lambda)$'s obtained from TI for the two-charge distributions follow closely their Gaussian approximations, and their derivatives depend linearly on λ .

On the contrary, results from the electronic polarization model (labeled $\mathcal{G} + \mathcal{D}$ in the table) show a clear deviation, larger than the error bar, of the (ΔG_{Gauss})'s with respect to their corresponding ΔG_{TI} . This is true for both charging processes considered here and also at lower temperature.

For the $\mathcal{G} + \mathcal{D}$ model, the derivatives $\partial G(\lambda)/\partial \lambda$ are very near linearity for both BChl-1 and BChl-2 (data not shown). Indeed, the Pearson's correlation coefficient is ~ 1 for the points from both models. Thus, the failure of the Gaussian approximation for the $\mathcal{G} + \mathcal{D}$ model is related to prediction of the slope of $\partial G(\lambda)/\partial \lambda$ versus λ from fluctuations at $\lambda = 0$. Calculation of the solvation free energy in the Gaussian approximation at $\lambda = 0.5$ and $\lambda = 1$ did not improve significantly the agreement with TI (results not shown). This behavior might be related to the

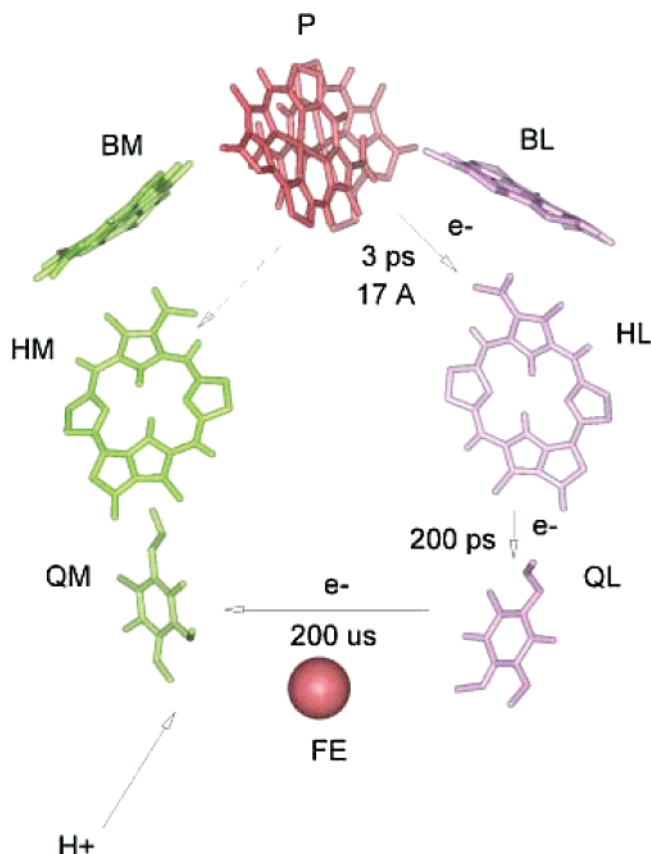


Figure 2. Arrangement of the cofactors in the photosynthetic reaction center of *Rb. sphaeroides*. Arrows show the electron-transfer pathways. P is the special pair composed of two bacteriochlorophylls, B's are the accessory bacteriochlorophylls, H's are bacteriopheophytins, and Q's are the two ubiquinones.

many-body nature of the dipolar interaction for which the central limit theorem cannot in principle be applied.

As stated in section II.D., charge rescaling was used to obtain the solvent charges for the polarizable model from the fixed charge model. This scheme should work well at least in a homogeneous system such as ours, since electronic polarizations can be well described by a mean field model. Indeed, Table 1 shows an excellent agreement between results for the two electrostatic models obtained via TI. An overall deviation of ~ 0.7 kcal mol $^{-1}$ is found, i.e., less than the statistical error. This is true for both charge distribution models of BChl.

At low temperature ($T = 200$ K) for a frozen system, the deviation for the two electrostatic models is larger than for the liquid, although still within the error bar. Thus, this result seems to indicate that this agreement between the two electrostatic models will break down for largely inhomogeneous systems. Confirmation for this finding is obtained in the investigation of electron transfer in a RC center protein discussed in the next section.

IV.B. Driving Forces in a Bacterial Reaction Center. In bacteria, RC proteins—simpler in structure and functions than those of plants—are located in the cellular membrane and sustain the first steps of photosynthesis. The RC protein of purple bacteria is composed of three principal subunits, called L, M, and H. The L and M proteins bind in their interior several cofactors arranged with a quasi-symmetry C_2 axis defined from the special pair P, a bacteriochlorophyll dimer, to the nonheme iron, as depicted in Figure 2. In *Rb. sphaeroides*, these cofactors are four bacteriochlorophylls (B) and two bacteriopheophytins

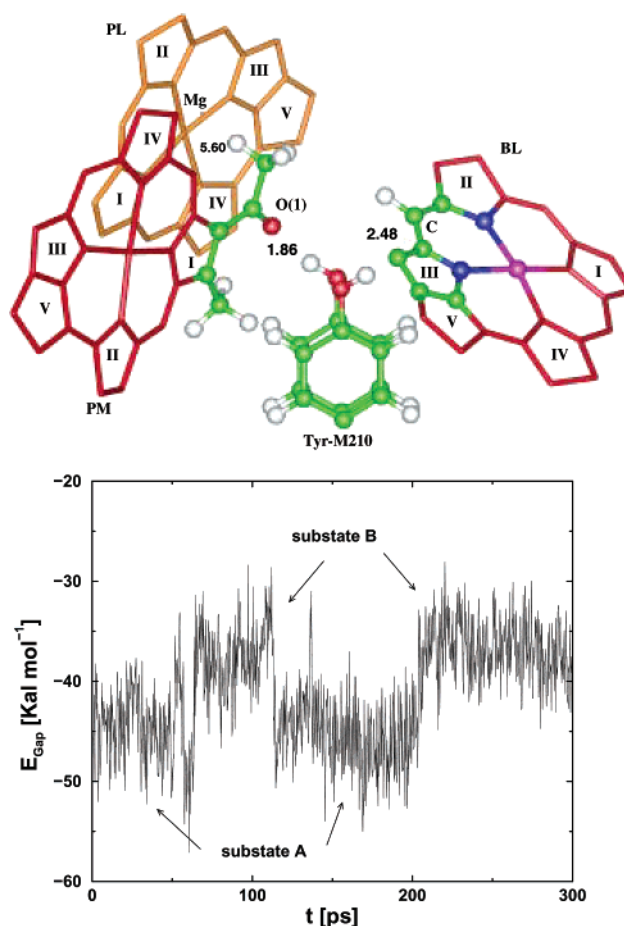


Figure 3. Conformational states coupled to the electron transfer $P \rightarrow B_L$. In the top panel, the position of the Tyr-M210 for the two possible orientations of the O—H group is depicted. Only the special pair P and the accessory bacteriochlorophyll B_L are shown. Atoms at less than 5 Å from the O—H group are represented as balls and sticks. In the bottom panel, the energy gap $\epsilon = U(1) - U(0)$ for one trajectory at $\lambda = 0$. The energy gap was computed for charge distribution RC-1 and the fixed charge model. The energy gap is kcal mol $^{-1}$.

(H) of type *a*, and two ubiquinones (U). The primary charge separation occurs after the initial photoexcitation of the special pair to P^* , when the excited electron moves to the bacteriopheophytin of the L side (H_L) covering 17 Å in ~ 3 ps.

We focus here on the electron transfer from P^* to the BChl on the L side (B_L), which is crucial to the understanding of the microscopic mechanism of the primary charge separation. The position of B_L with respect to P^* in the energy scale is believed to discriminate between a one-step or two-step mechanisms. In the latter, the B_L^- is a real intermediate state while in the former it is only virtually affecting the electronic coupling between initial and final states.

In a recent work, Ceccarelli and Marchi¹¹ have shown that the local dynamics of the residue Tyr-M210 can significantly affect the free-energy surfaces of an electron transfer from P^* to B_L . Indeed, a bistate distribution of the energy gap was observed which correlates to the two stable orientations of the OH group of Tyr-M210. This behavior is also found by our simulation, as shown in Figure 3, where the history of the energy gap is plotted as obtained for the initial state with the RC-1 charge distribution. Although Figure 3 shows results for the fixed charges electrostatic model, the E-gap computed with explicit electronic polarization behaves similarly. Thus, two different states are observed: in substate **A** the OH group is pointing toward B_L and in substate **B** OH is oriented toward P.

TABLE 2: Solvation Free Energies for the Electron Transfer from P to B_L Obtained with the Charge Distribution RC-1^a

models	ϵ	σ^2	ΔG Gauss	ΔG TI	$ G_{\text{TI}} - G_{\text{Gauss}} $
AB (\mathcal{G})				-53.5 ± 0.6	
A (\mathcal{G})	-44.9 ± 0.9	11.2 ± 3.6	-53.9 ± 3.0	-53.9 ± 0.6	0.4
B (\mathcal{G})	-36.8 ± 0.6	8.8 ± 9.0	-44.2 ± 2.1	-53.1 ± 0.6	8.9
AB ($\mathcal{G} + \mathcal{D}$)				-51.6 ± 0.6	
A ($\mathcal{G} + \mathcal{D}$)	-46.2 ± 0.6	4.4 ± 1.5	-49.9 ± 1.2	-51.9 ± 0.6	2.1
B ($\mathcal{G} + \mathcal{D}$)	-40.8 ± 0.6	3.3 ± 0.6	-43.6 ± 0.6	-52.3 ± 0.6	8.7

^a The Gaussian free energy and the Gaussian parameters, the mean (ϵ) and the width (σ^2), are reported for two different electrostatic models, (\mathcal{G}) and ($\mathcal{G} + \mathcal{D}$) discussed in the text. The labels A and B refer to the substates of the RC as discussed in the text, whereas AB is the statistical average of the two. Statistical errors were obtained by block averages and are 3 times the standard deviation. Energies are in kcal mol⁻¹.

TABLE 3: Solvation Free Energies for Electron Transfer from P to B_L Obtained with the Charge Distribution RC-2^a

models	ϵ	σ^2	ΔG Gauss	ΔG TI	$ G_{\text{TI}} - G_{\text{Gauss}} $
AB (\mathcal{G})				-57.8 ± 0.6	
A (\mathcal{G})	-50.4 ± 0.9	10.2 ± 3.0	-58.9 ± 2.7	-58.1 ± 0.6	0.8
B (\mathcal{G})	-43.1 ± 0.6	7.9 ± 1.5	-49.7 ± 1.5	-57.4 ± 0.6	7.7
AB ($\mathcal{G} + \mathcal{D}$)				-54.5 ± 0.6	
A ($\mathcal{G} + \mathcal{D}$)	-50.1 ± 0.3	4.1 ± 1.5	-53.8 ± 1.5	-54.8 ± 0.6	1.0
B ($\mathcal{G} + \mathcal{D}$)	-44.9 ± 0.6	3.3 ± 0.6	-47.6 ± 0.6	-54.2 ± 0.6	6.6

^a See Table 2 and text for explanation. Energies are in kcal mol⁻¹.

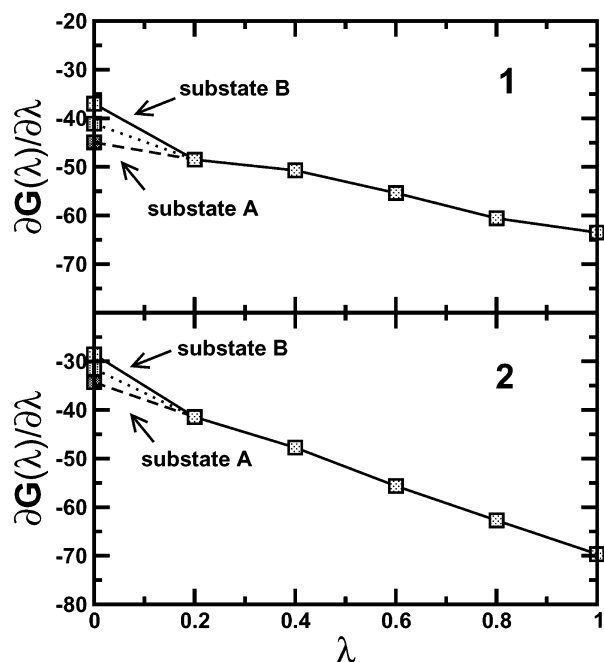


Figure 4. Derivative of the free-energy vs the charging parameter λ for the electron transfer $PB_L \rightarrow P^+B_L^-$. Results are presented on panels 1 and 2 for the fixed charge model and the model with electronic polarization, respectively. The charge distribution RC-1 was used. All energies are given in kcal mol⁻¹.

We also label state AB the average value of E-gap at each instant.

This conformational transition breaks the linearity of the system response to the process. This is shown in Figures 4 and 5 where $\partial G/\partial \lambda$ as a function of λ is plotted for RC-1 and RC-2, respectively. The deviation from linearity is more visible in the points near $\lambda = 0$. Indeed, for points beyond $\lambda = 0.2$ and for both distributions the population of substate B disappears. For distribution RC-1 the transition to a single state occurs already at $\lambda = 0.2$, and for RC-2 at $\lambda = 0.2$ the population of substate B is less than 5%.

Thus, this nonlinearity of the solvent coupling to ET affects little the calculation of the driving force by TI. Indeed, Tables 2 and 3, where the driving force for the reaction $P^*B_L \rightarrow P^+B_L^-$ is reported, show that differences in free energies among substates A, B, and AB are <0.7 kcal mol⁻¹.

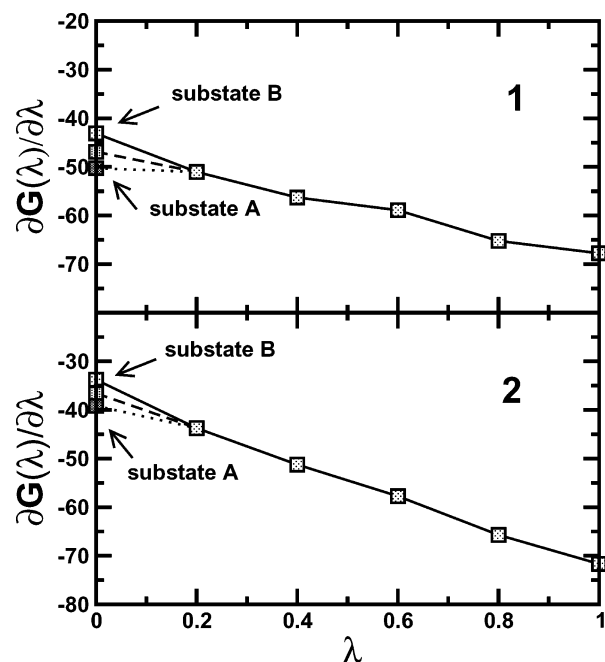


Figure 5. Same as in Figure 4 except that the charge distribution RC-2 was used.

The existence of a bistate distribution in the ensemble at $\lambda = 0$ prevents the straightforward use of the Gaussian approximation to obtain estimates of the driving force through eq 4. As was done in ref 11, the energy gap data can be divided among the two substates A and B, and the statistics can be computed separately.

For the electrostatic model \mathcal{G} and for energy gap statistics obtained in A in the initial state $\lambda = 0$, we can obtain driving force estimates very close to those computed from the TI scheme (see Table 4). Indeed, in this case the orientation of the OH bond is unchanged if λ is increased. On the other hand, since the orientation of OH does change going from substate B and increasing λ , the Gaussian approximation driving force obtained from data in that state has a much larger deviation from the TI value. In confirmation to our findings for the case of a hydrated bacteriochlorophyll, Gaussian approximation results obtained from model $\mathcal{G} + \mathcal{D}$ do not work very well for both charge distributions, although they do work better for RC-2.

TABLE 4: Ionization and Affinity Energies (kcal mol⁻¹) for Isolated Chromophores of *Rb. sphaeroides* Calculated, Taken from Ref 26

system	ionization	affinity
P	130.5	
P*	97.5	
BChl		-50.7
BPh		-47.9
P* + his	91.3	
BChl + his		-42.2

TABLE 5: Driving Force for the Electron Transfer from P to B_L Obtained with the Charge Distributions RC-1 and RC-2^a

RC-1 charge distribution		RC-2 charge distribution	
model	ΔG° [kcal mol ⁻¹]	model	ΔG° [kcal mol ⁻¹]
AB (\mathcal{G}) (TI)	-6.7 \pm 0.6	AB (\mathcal{G}) (TI)	-11.0 \pm 0.6
A (\mathcal{G}) (TI)	-7.0 \pm 0.6	A (\mathcal{G}) (TI)	-11.3 \pm 0.6
B (\mathcal{G}) (TI)	-6.1 \pm 0.6	B (\mathcal{G}) (TI)	-10.6 \pm 0.6
A (\mathcal{G}) (Gauss)	-7.2 \pm 3.0	A (\mathcal{G}) (Gauss)	-12.7 \pm 2.4
B (\mathcal{G}) (Gauss)	2.3 \pm 2.1	B (\mathcal{G}) (Gauss)	-2.7 \pm 1.5
AB ($\mathcal{G} + \mathcal{D}$) (TI)	-4.8 \pm 0.6	AB ($\mathcal{G} + \mathcal{D}$) (TI)	-7.7 \pm 0.6
A ($\mathcal{G} + \mathcal{D}$) (TI)	-5.1 \pm 0.6	A ($\mathcal{G} + \mathcal{D}$) (TI)	-7.9 \pm 0.6
B ($\mathcal{G} + \mathcal{D}$) (TI)	-4.5 \pm 0.6	B ($\mathcal{G} + \mathcal{D}$) (TI)	-7.4 \pm 0.6
A ($\mathcal{G} + \mathcal{D}$) (Gauss)	-3.1 \pm 1.2	A ($\mathcal{G} + \mathcal{D}$) (Gauss)	-7.0 \pm 1.5
B ($\mathcal{G} + \mathcal{D}$) (Gauss)	3.2 \pm 0.6	B ($\mathcal{G} + \mathcal{D}$) (Gauss)	-0.8 \pm 0.6

^a Labeling of the results is the same as in Table 2. Driving forces marked (TI) and (Gauss) were computed by thermodynamic integration and Gaussian approximation, respectively. Statistical errors were obtained by block averages and are 3 times the standard deviation. Energies are in kcal mol⁻¹.

Tables 2 and 3 also show that the Gaussian widths for model $\mathcal{G} + \mathcal{D}$ are between 1.5 and 1.6 times smaller than that for model \mathcal{G} . This is not unexpected as the optical dielectric constant for dense fluids is known to be around 2.

To obtain the effective driving force for the reaction, one has to add the contribution for the gas-phase ionization and the affinity. As in a previous study,¹¹ the values of these energies were estimated by DFT calculation and taken from literature (see Table 4). The driving forces computed with various models are summarized in Table 5. Here, we notice large deviations between TI and Gaussian approximations in the substate B, while driving forces obtained from weighted average results from substates A and B are far away from the TI driving forces. Our simulations gave a relative occupancy of the two substates around 50%.

Also noticeable is that the deviations between results obtained with the \mathcal{G} and $\mathcal{G} + \mathcal{D}$ models are larger here than those obtained for the hydrated BChl. As expected, the heterogeneity of the environment is in this case much more important. We also find that charge distribution RC-2 always produces more negative driving forces.

IV.C. Free-Energy Surfaces in a Bacterial Reaction Center. The activation free energy is the work done by the fluctuations of the solvent to get the system in the transition state. We have obtained this quantity by computing directly the free-energy surfaces for electron transfer by the so-called WHAM procedure. These free-energy profiles are shown in Figure 6 for the RC-1 and RC-2 distributions.

We first notice that in all cases the surface corresponding to the initial state (on the right-hand side of each panel) is wider than the surface associated to the final state. This is due to the coupling of the bistable state with the energy gap. In the case of distribution two minima are observed: well resolved for the $\mathcal{G} + \mathcal{D}$ electrostatic model with a barrier of about $\sim 1 k_B T$, more

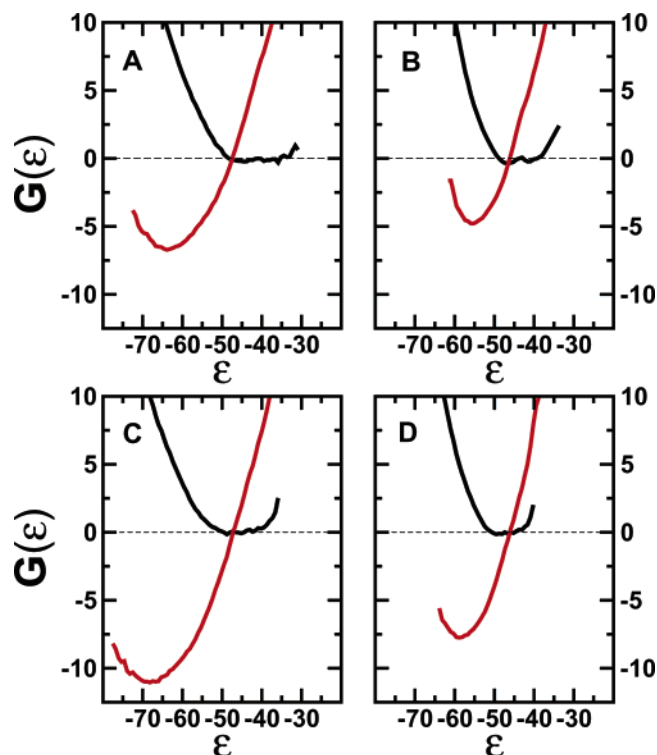


Figure 6. Free-energy surfaces for the $PB_L \rightarrow P^+B_L^-$ electron transfer. On the abscissa is the energy gap, or ϵ , and on the ordinate the system free energy, or $G(\epsilon)$, is shown (in kcal mol⁻¹). Results obtained with the charge distribution RC-1 are shown on panel A, the fixed charge model, and panel B, the electronic polarizable model. Data obtained with charge distribution RC-2 are instead displayed on panel C, the fixed charge model and panel D, the electronic polarizable model. The average value of the reactant state minima are always shifted to zero in the free-energy scale.

shallow for the \mathcal{G} model. For charge distribution RC-1 the initial states show only large shallow minima. This free-energy structure of the initial neutral state for the two models is related to the overlap of the energy gap explored by the system in substates A and B. This overlap is, in our calculation, larger for distribution RC-2 and smaller for RC-1.

By visually inspecting Figure 6, the activation free energies, or G^* 's, are in all cases less than 0.2 of kcal mol⁻¹. For distribution RC-1 and electrostatic model $\mathcal{G} + \mathcal{D}$, the internal barrier of the initial state is of ~ 0.6 kcal mol⁻¹ or $1 k_B T$ at 300 K. We notice that G^* 's computed by Gaussian approximation within A are also very close to zero. On the contrary, for B a large activation energy is found, in all cases near 3 kcal mol⁻¹.

Finally, we observe that for model \mathcal{G} the free-energy surfaces of the final state (on the left-hand side in Figure 6) are larger than those obtained, including electronic polarization. This is a consequence of the polarizable dipoles exerting a larger screening on the electrostatic field acting on the redox sites.

V. Conclusions

In a previous investigation,^{10,11} we have used linear response theory to compute the kinetic parameters of the primary charge separation of bacterial photosynthesis. In this paper, we have tested the Gaussian approximation for the energy gap probability distributions at the base of linear response. From the simulation of a BChl in solution, we have shown that the Gaussian approximation is not satisfied if electronic polarization is explicitly included in the electrostatic model. We find that the deviation between solvation free energies obtained with the

Gaussian approximation and TI is small, but larger than the statistical error.

As in a previous study,¹¹ the charges used in the $G + \mathcal{O}$ model of this paper were obtained by multiplying those of the G model by a factor of 0.8. This choice of scaling factor has shown to be appropriate for isotropic systems such as the hydrated BChl, as the computed solvation free energies for the G and $G + \mathcal{O}$ models are in very good agreement with each other. We verified that differences between the two models arise for electron transfer in the RC protein where anisotropy of the milieu is important.

Nonlinearities in the coupling between the environment and the exchanged electron produce a large effect on the corresponding diabatic free-energy surfaces. We have shown that the isomerization of the Tyr-M210, implying two substates, A and B, affects the initial state of the electron exchange between special pair P and the accessory bacteriochlorophyll B_L and produces a shallow free-energy well for the P*B_L state. As a result, the activation free energy for this reaction, crucial to the mechanism of the primary charge separation, is lowered with respect to the Gaussian approximations for substates A and B. For charge distribution RC-1 the free-energy surface of the initial state shows two minima separated by a small barrier of $< 1 k_B T$.

Finally, our study has shown that electronic polarization crucially screens the dielectric response of the systems. Indeed, the curvature of the free-energy surfaces, the inverse of which is related to the reorganization energy, is more than twice as small for fixed charges than for induced dipoles. This is to be expected given that the optical dielectric constant is always close to two for most dense fluids.

To conclude and summarize, this paper has investigated linear response for treating electron transfer in complex biomolecules with and without explicit electronic polarization. The limits of this approximation and the size of its deviation from results obtained with thermodynamic integration, in principle exact, have been pinpointed. These findings will be of crucial importance in further investigations of electron transfer in complex biomolecules making use of linear response, still the easiest and least time-consuming approach.

Acknowledgment. F.S. acknowledges a research grant from the Fondazione Angelo Della Riccia obtained in 2003.

References and Notes

- (1) Kuznetsov, A.; Ulstrup, J. *Electron Transfer in Chemistry and Biology*. Wiley Series in Theoretical Chemistry; John Wiley and Sons: New York, 1999.
- (2) Marcus, R. A.; Sutin, N. *Biochim. Biophys. Acta* **1985**, *811*, 265–322.
- (3) Marcus, R. A. *Annu. Rev. Phys. Chem.* **1964**, *15*, 155–196.
- (4) Chandler, D. In *Classical and Quantum Dynamics in Condensed Phase Simulations*; Berne, B., Ciccotti, G., Coker, D., Eds.; World Scientific: Singapore, 1998; pp 29–49.
- (5) Simonson, T. *Proc. Natl. Acad. Sci. U.S.A.* **2002**, *99*, 6544–6549.
- (6) Frenkel, D.; Smith, B. *Understanding Molecular Simulation*. Academic Press: San Diego, CA, 1996.
- (7) Chelli, R.; Procacci, P. *J. Chem. Phys.* **2002**, *117*, 9175.
- (8) Zhou, R.; Berne, B. J.; Germain, R. *Proc. Natl. Acad. Sci. U.S.A.* **2001**, *98*, 14931.
- (9) Frauenfelder, S. G. S.; Wolynes, P. G. *Science* **1991**, *254*, 1598–1603.
- (10) Ceccarelli, M.; Marchi, M. *J. Phys. Chem. B* **2003**, *107*, 1423–1431.
- (11) Ceccarelli, M.; Marchi, M. *J. Phys. Chem. B* **2003**, *107*, 5630–5641.
- (12) Warshel, A.; Parson, W. W. *Q. Rev. Biophys.* **2001**, *34*, 563–679.
- (13) Torrie, G. M.; Valleau, J. P. *Chem. Phys. Lett.* **1974**, *28*, 578–581.
- (14) Roux, B. *Comput. Phys. Commun.* **1995**, *91*, 275–282.
- (15) Darden, T.; Pearlman, D.; Pedersen, L. G. *J. Chem. Phys.* **1998**, *109*, 10921–10935.
- (16) Kumar, S.; Bouzida, D.; Swendsen, R. H.; Kollman, P. A.; Roseberg, J. M. *J. Comput. Chem.* **1992**, *13*, 1011–1021.
- (17) Thole, B. T. *Chem. Phys.* **1981**, *59*, 341–350.
- (18) van Duijnen, P. T.; Swart, M. *J. Phys. Chem A* **1998**, *102*, 2399–2407.
- (19) Toukmaji, A.; Sagui, C.; Board, J.; Darden, T. *J. Chem. Phys.* **2000**, *113*, 10913–10927.
- (20) Jorgensen, W. L.; Chandrasekhar, J.; Madura, J. D.; Impey, R. W.; Klein, M. L. *J. Chem. Phys.* **1983**, *79*, 926.
- (21) Ceccarelli, M.; Procacci, P.; Marchi, M. *J. Comput. Chem.* **2003**, *24*, 129.
- (22) Procacci, P.; Paci, E.; Darden, T.; Marchi, M. *J. Comput. Chem.* **1997**, *18*, 1848–1862.
- (23) Essmann, U.; Perera, L.; Berkowitz, M. L.; Darden, T.; Lee, H.; Pedersen, L. G. *J. Chem. Phys.* **1995**, *103*, 8577–8593.
- (24) Hummer, G.; Pratt, L. R.; García, A. E. *J. Phys. Chem.* **1996**, *100*, 1206–1215.
- (25) Hummer, G.; Pratt, L. R.; García, A. E. *J. Am. Chem. Soc.* **1997**, *119*, 8523–8527.
- (26) Blomberg, M. R. A.; Siegbahn, P. E. M.; Babcock, G. T. *J. Am. Chem. Soc.* **1998**, *120*, 8812–8824.